Comparison of Transient Performances for Synchronous and Eddy-current Torque Couplers

Thierry Lubin, Julien Fontchastagner, Smail Mezani, Abderrezak Rezzoug

Comparison of Transient Performances for Synchronous and Eddy-current Torque Couplers

Thierry Lubin, Julien Fontchastagner, Smail Mezani, and Abderrezak Rezzoug

***Abstract* -- In this paper, we compare the transient performances of synchronous and eddy-current magnetic couplings. Based on a two-dimensional approximation for the magnetic field distribution, closed-form expressions for the transmitted torque are first presented. The torque formulas are then used to study the transient responses during a start-up and for a sudden application of a load torque. Simulation results are compared with those obtained from tests. It is shown that overload torque condition leads to the loss of synchronism for the synchronous coupling. A discussion about the benefits and the disadvantages of each topology in terms of transient responses is given.**

***Index Terms*-- Analytical model, eddy-current, magnetic transmission, torque, transient performance,**

I. Introduction

MAGNETIC couplings can transmit a torque from a primary driver to a follower without mechanical contact. As the torque could be transmitted across a separation wall, magnetic couplings are well suited for use in isolated systems. Compared to mechanical couplings, magnetic couplings present many advantages such as intrinsic protection against overloads, reduced maintenance, and a high tolerance to misalignment between the prime mover and the load. There are two main types of magnetic torque couplers: synchronous [1]-[14] and asynchronous (eddy-current) [15]-[25], both with radial or axial flux topologies. In this paper, we focus on magnetic couplings with axial-field topology also called face to face magnetic couplings.

The synchronous magnetic coupling under study is shown in Fig. 1. It consists of two similar rotors (discs) made from soft iron yokes on which sector-shaped NdFeB permanent magnets (PMs) are glued and arranged to obtain alternately north and south poles. The torque production results from the magnetic field interaction in the air-gap which separates the two discs. Hence, the torque applied to one disc is transferred through the air-gap to the other disc. As shown in Fig. 1, the geometrical parameters of the studied magnetic coupling are the inner and outer radii of the magnets R_1 and R_2, the air gap length e, and the magnets thickness h. The pole-arc to pole-pitch ratio of the permanent magnets is α. The number of pole-pairs is p. The values of geometrical parameters for the prototype are given in Table I. With these parameters we obtain a maximum transmissible torque of 60Nm for an air-gap of 4mm [6].

The geometry of the eddy-current magnetic coupling is shown in Fig. 2. It consists of two disks:

- one disc is composed of NdFeB PMs glued on a soft-magnetic yoke (similar to the synchronous coupler);
- the other disc is equipped with a conducting plate (copper) also fixed on an iron yoke

The working principle of eddy-current couplings is well known [15]. Let us note Ω_1 the PMs disc rotating speed and Ω_2 the copper rotor speed. Due to the slip speed ($\Omega=\Omega_1-\Omega_2$), eddy currents are induced in the conducting plate. These currents interact with the PMs magnetic field to generate a torque. The usual operation of such a device corresponds to low-slip values as to limit the temperature rise, due to the induced-currents. The geometrical parameters of the prototype are given in Table II. With these parameters and considering e = 3 mm for the air-gap, we obtain a torque of about 10 Nm for a slip speed of 150 rpm [21].

The purpose of this paper is to compare the transient performance of synchronous and eddy-current couplings. Simple analytical expressions for the transmitted torque are presented first. The torque formulas are then used to study the transient responses during a start-up and for a sudden application of load torque. The simulation results are compared with those obtained from tests. The benefits and the disadvantage of each topology in terms of transient responses are discussed.

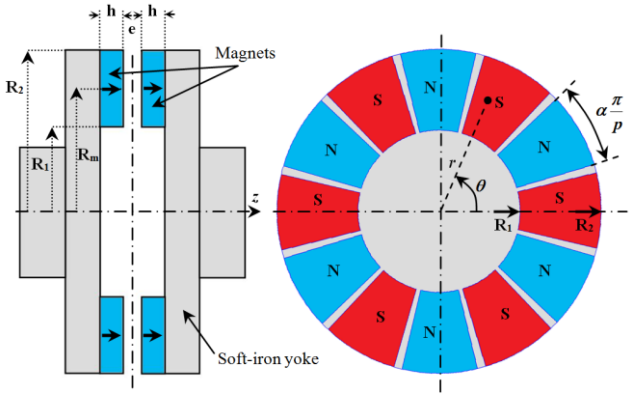

Fig. 1. Geometry of axial-field synchronous magnetic coupling (p = 6).

TABLE I
PARAMETERS OF THE SYNCHRONOUS-TYPE COUPLER

Symbol	Quantity	value
R_1	Inner radius of the magnets	30 mm
R_2	Outer radius of the magnets	60 mm
R_e	Mean radius of the magnets	45 mm
h	Magnets thickness	7 mm
e	Air-gap length	variable
α	PMs pole-arc to pole-pitch ratio	0.9
p	Pole-pairs number	6
B_r	Remanence of the permanent magnets	1.25 T

T. Lubin, J. Fontchastagner, S. Mezani, and A. Rezzoug are with the Groupe de Recherche en Electrotechnique et Electronique de Nancy (GREEN), Université de Lorraine, 54506 Vandoeuvre-lès-Nancy, France (e-mail: thierry.lubin@univ-lorraine.fr).

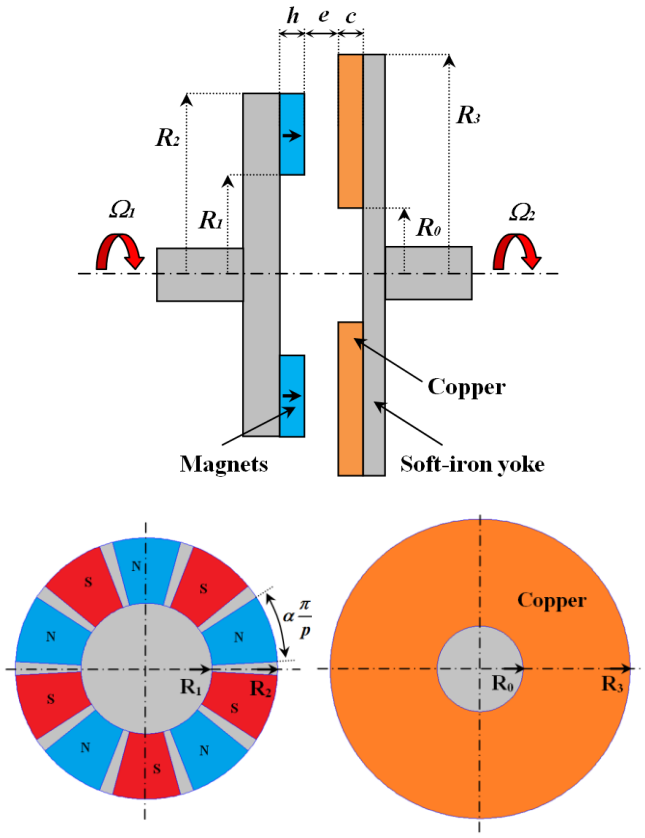

Fig. 2. Geometry of axial-field eddy-current magnetic coupling (p = 5).

TABLE II
PARAMETERS OF THE EDDY-CURRENT TYPE COUPLER

Symbol	Quantity	value
R_1	Inner radius of the magnets	30 mm
R_2	Outer radius of the magnets	60 mm
R_0	Inner radius of the conducting plate	15 mm
R_3	Outer radius of the conducting plate	75 mm
h	Magnets thickness	10 mm
e	Air-gap length	variable
c	Conducting plate thickness	5 mm
α	PMs pole-arc to pole-pitch ratio	0.9
p	Pole-pairs number	5
B_r	Remanence of the permanent magnets (NdFeB)	1.25 T
σ	Conductivity of the conducting plate (copper)	57 MS/m

Fig. 3 shows the pictures of the synchronous and eddy-current magnetic coupling prototypes placed on the test bench. In order to make comparisons in terms of transient performance, we have used the same test bench for the two couplings. The magnetic couplings are inserted between two similar DC machines (3kW, 3000 rpm) as shown in Fig. 3.

II. TORQUE FORMULAS

Analytical modeling of axial-field magnetic couplings is a difficult task because of the three-dimensional nature of the magnetic field distribution [14], [25]. To obtain simple expressions for the torque, the 3D problem can be reduced to a 2D one. A cylindrical cutting surface at the mean radius of the magnets $R_m=(R_1+R_2)/2$ is used to compute the magnetic field [6], [19], [21].

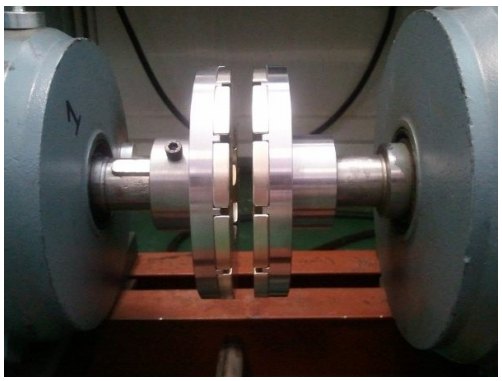

(a)

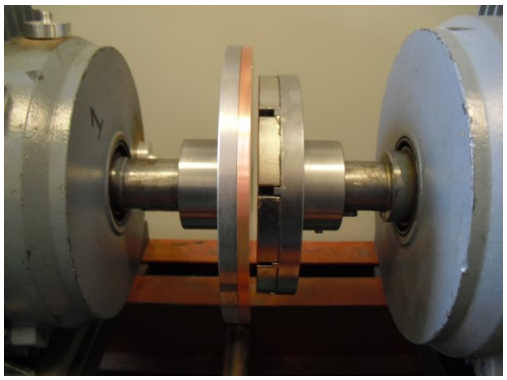

(b)

Fig. 3. Axial-field magnetic coupling prototypes placed on the same test bench. (a): Synchronous coupling; (b): Eddy-current coupling.

With this approximation, we neglect the edge effects in the radial direction for the magnetic field distribution. Therefore, a correction factor should be involved with the 2D models for both the synchronous and eddy current couplings in order to get precise torque prediction [13], [19]. Moreover and for simplicity reasons, the following assumptions are adopted:

1) infinite magnetic permeability and zero conductivity is assumed for the iron yokes;

2) the first space harmonic is only considered for the magnetic field distribution;

3) the PMs are axially magnetized with relative recoil permeability $\mu_r = 1$ (rare-earth magnets are used) and zero conductivity;

4) for the eddy-current coupling, the reaction field due to the induced currents is neglected because of the low-slip assumption (normal operation for this device).

A. Synchronous magnetic coupling

Fig. 4 shows the resulting 2D model for the synchronous magnetic coupling. This simplification makes the axial magnetic coupling equivalent to a linear magnetic coupling where δ (torque angle) is the relative angular position between the magnets of region I and region III. Detailed mathematical derivations for the magnetic field calculation in the different regions can be found in [6] and will not be repeated here. We have shown that applying the previous assumptions leads to a simple expression for the torque which depends directly on the physical and geometrical parameters given in Table I.

$$T = T_{\max} \sin(p\delta) \tag{1}$$

with

$$T_{\max} = \frac{16}{3\pi} k_c \frac{B_r^2}{\mu_0} R_2^3 \left(1 - \left(\frac{R_1}{R_2}\right)^3\right) \sin^2\left(\alpha \frac{\pi}{2}\right) \frac{\sinh^2(a)}{\sinh(2(1+\nu)a)} \tag{2}$$

$$a = p\frac{h}{R_m} \quad ; \quad \nu = \frac{e}{2h} \quad ; \quad k_c = 0.75 \tag{3}$$

where k_c is a 3D correction factor which was determined in [13] from a parametric study. Fig. 5 shows a comparison between the torque measurements and the predicted values obtained using (1)-(2). We have considered four values for the air-gap. It can be observed that good agreements are obtained whatever the air-gap value if we consider the 3D correction factor in the torque formula.

B. Eddy-current magnetic coupling

Fig. 6 shows the 2D model of the eddy-current coupling. The whole domain of the field problem is divided into three regions: the PMs region (region I), the air-gap region (region II), and the copper region (region III). As the reaction field is neglected, the air-gap and copper regions can be connected because we have the same governing equation for this region. Detailed derivation for the magnetic field calculation in each region is given in [21]. The induced current density in the conducting plate can be obtained from the Lorentz equation. A closed-form expression for the electromagnetic torque is then derived:

$$T = K\Omega = K(\Omega_1 - \Omega_2) \tag{4}$$

with

$$K = \frac{8}{\pi} k_{Russel} \sigma B_r^2 R_m^3 Lc \sin^2\left(\alpha \frac{\pi}{2}\right) \times \frac{\sinh^2(\beta h)}{\sinh^2(\beta(h+e+c))} \left(1 + \frac{\sinh(2\beta c)}{2\beta c}\right) \tag{5}$$

and

$$k_{Russel} = 1 - \frac{(2/\beta L)\tanh(\beta L/2)}{1 + \tanh(\beta L/2)\tanh(\lambda\beta L/2)} \quad ; \quad \beta = p/R_m \tag{6}$$

$$\lambda = (H - L)/L \quad ; \quad L = R_2 - R_1 \quad ; \quad H = R_3 - R_0$$

As expected for low-slip values, the torque is proportional to the slip speed Ω ($rad.s^{-1}$). To take into account the 3D effects, an effective correction factor noted k_{Russel} is used [26]. Fig. 7 shows a comparison between the analytically predicted torque-slip speed characteristics and the measured data for three values of the air-gap length. It can be seen that the measured and computed torques are in good agreement. Indeed, the relative difference between the analytical and the test results does not exceed 10%. This difference is larger when the slip speed increases. This difference is due to the well-known reaction field which can no longer be ignored for a slip speed greater than 200 rpm for the studied coupling.

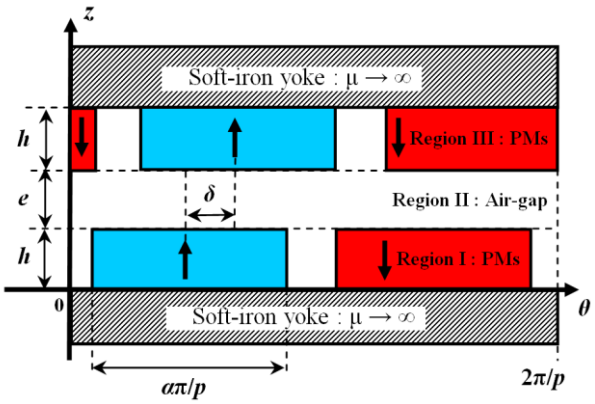

Fig. 4. 2-D model of the synchronous magnetic coupling at the mean radius R_m

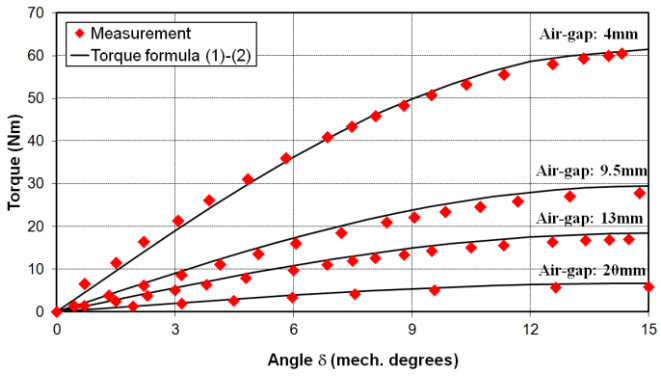

Fig. 5. Measured and computed torque versus the angular displacement δ for four values of the air-gap length (synchronous coupling).

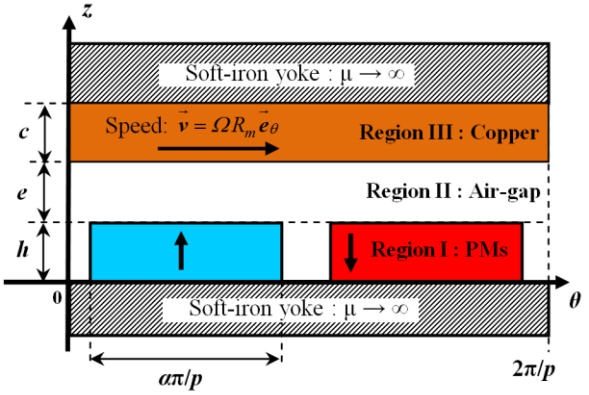

Fig. 6. 2-D model of the eddy-current coupling at the mean radius R_m.

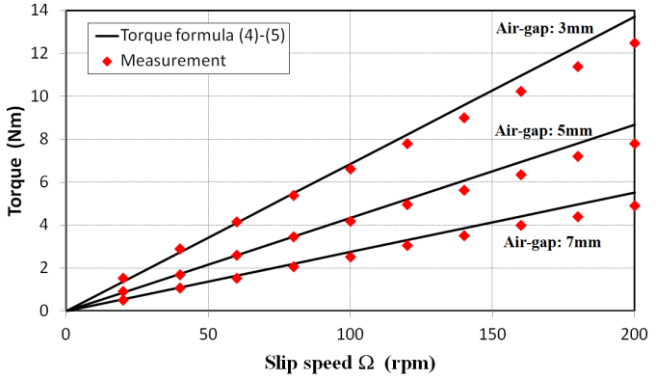

Fig. 7. Measured and computed torque-slip speed characteristics for three values of the air-gap length (eddy-current coupling).

III. TRANSIENT ANALYSIS

While the steady-state performance of magnetic couplings are widely studied in the literature, little attention is given to transient performance [8], [16] and experimental data are practically nonexistent [13], [21]. However, the transient behavior of a magnetic coupling has a great impact in most practical applications like servomechanisms. For engineering purposes, it is important to have an effective tool to predict the consequence of using a magnetic coupling under transient operation.

Fig. 8 shows the test bench arrangement for the transient analysis. The magnetic coupling (synchronous or eddy-current) is placed between two DC motors. One motor is used as the prime mover. The speed is controlled by changing the voltage applied to the armature of the DC motor. A DC generator is used to apply a load torque by connecting a resistance to its armature winding terminals. The DC motor rotates at Ω_1 and the load runs at Ω_2. Two encoders (4096 pulses/revolution) have been placed on the test bench to measure the angular position and speed on both sides of the coupling during the transient.

The transient analysis of the system is obtained from the classical equation of motion for rotating rigid bodies:

$$\begin{aligned} J_1 \frac{d\Omega_1}{dt} + B_1\Omega_1 &= T_{DC} - T \\ J_2 \frac{d\Omega_2}{dt} + B_2\Omega_2 &= T - T_{load} \end{aligned} \tag{7}$$

where J_1 and B_1 denote the moment of inertia and the viscous damping coefficient on the DC motor side (prime mover), J_2 and B_2 denote the moment of inertia and the viscous damping coefficient of the load, as indicated in Fig. 8. T_{DC} is the DC motor torque, T_{load} is the external load torque, and T is the torque transmitted by the magnetic coupling.

A. Synchronous magnetic coupling

The transmitted torque (1) for the synchronous magnetic coupling can be re-written as follows

$$T = T_{\max}\sin(p\delta) = T_{\max}\sin\left(p(\theta_1 - \theta_2)\right) \tag{8}$$

where $\Omega_1 = d\theta_1/dt$ and $\Omega_2 = d\theta_2/dt$.

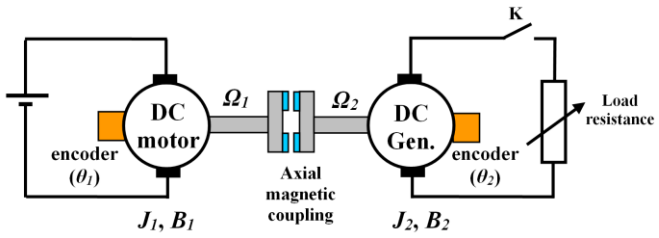

Fig. 8. Test bench arrangement for transient analysis of magnetic coupling.

If we consider small variations for the load angle δ, we obtain the approximate linear equation:

$$T = pT_{\max}(\theta_1 - \theta_2) = k(\theta_1 - \theta_2) \tag{9}$$

where k is the torsional stiffness (in Nm.rad^{-1}). The torsional stiffness is equal to the initial slope of the torque vs. position curves shown in fig. 5. Its expression is easily obtained from (2). This coefficient depends on the geometrical parameters of the coupling and more particularly on the air-gap value e. Fig. 9 shows the variation of the torsional stiffness k versus the air-gap length, the other parameters are those given in Table I. As expected, k decreases with the air-gap length (the coupling is more elastic with a large air-gap). For an air-gap value of 4 mm, the torsional stiffness of the studied magnetic coupling is around 370 Nm.rad^{-1}. For comparison, rigid or semi-flexible mechanical couplings present a torsional stiffness of more than 5000 Nm.rad^{-1}.

From (7) and considering (9), we get a system of second-order linear differential equations for the angular positions θ_1 and θ_2

$$\begin{aligned} J_1 \frac{d^2\theta_1}{dt^2} + B_1 \frac{d\theta_1}{dt} + k\theta_1 &= T_{DC} + k\theta_2 \\ J_2 \frac{d^2\theta_2}{dt^2} + B_2 \frac{d\theta_2}{dt} + k\theta_2 &= k\theta_1 - T_{Load} \end{aligned} \tag{10}$$

The torsional stiffness k has a great impact on the damping ratio of the mechanical system and can be the cause of large oscillations on the speed response [10], [11], [13].

The transient start-up performance is assessed by running the DC motor from standstill (at t = 0s) to a speed of 400 rpm under no-load condition. Figure 10 shows the speed response for an air-gap value e =13 mm (k = 105 Nm.rad^{-1}). We have deliberately chosen a large value for the air-gap (small value for k) to highlight the speed oscillations.

The simulation results have been computed with (10). Experimental and simulation results show clearly that there are speed oscillations between the two rotors of the magnetic coupling. These oscillations are even more important when increasing the air-gap [13].

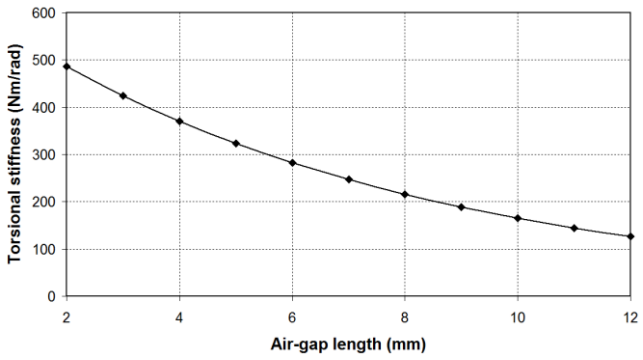

Fig. 9. Torsional stiffness coefficient k versus the air-gap length.

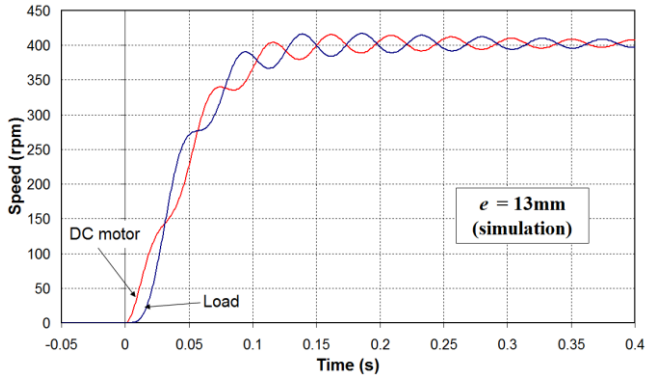

(a)

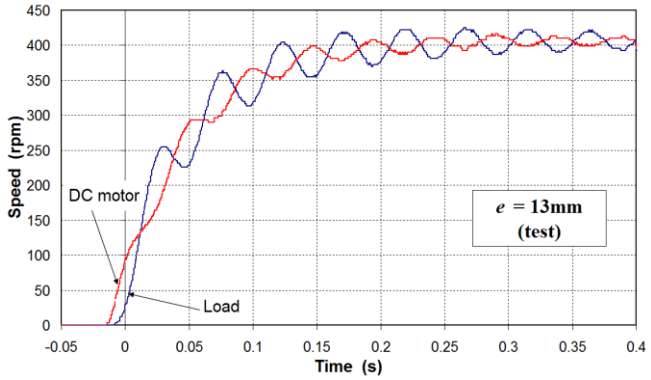

(b)

Fig. 10. Speed responses for the synchronous coupling (e = 13mm): (a) simulation result (b) experimental result.

The transient performance with a sudden application of a load torque is now studied. Before the load torque is applied, the DC motor is in steady-state condition and rotates with a speed of around 750 rpm (under no-load condition). A sudden load torque of 4Nm is then applied to the system at t = 0s. Fig. 11 shows the speed response. The transient regime lasts around 0.3s, after which the two speeds become stable and synchronous. Fig. 12 shows the speed responses (experimental results) that follow a sudden application of a load torque (13.5Nm ; e = 20mm) which is sufficient to cause the synchronism loss (overload condition). The speed of the DC motor is maintained at around 750 rpm (after some oscillations) while the load side of the coupling stops. This test clearly shows the overload self-protection of the magnetic coupling.

B. Eddy-current magnetic coupling

For the eddy-current coupling, we have assumed (4) that the torque transmitted by the magnetic coupling is proportional to the slip speed (small slip-value assumption). With this assumption, the eddy-current magnetic coupling can be seen as an additional viscous damping coefficient which is equal to the torque coefficient K given by (5).

Fig. 13 shows the variation of K versus the air-gap length (the other parameters are those given in table II). As expected, K decreases with the air-gap length. From (7) and considering (4), we get a system of first-order linear differential equations for the speeds:

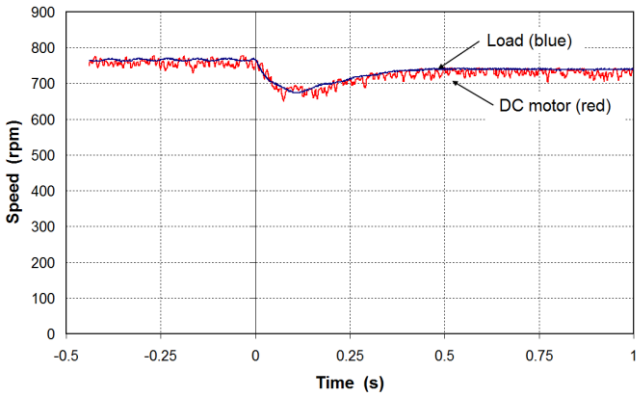

Fig. 11. Speed response to a sudden load torque of 4Nm for the synchronous coupling (experimental results, e = 20mm).

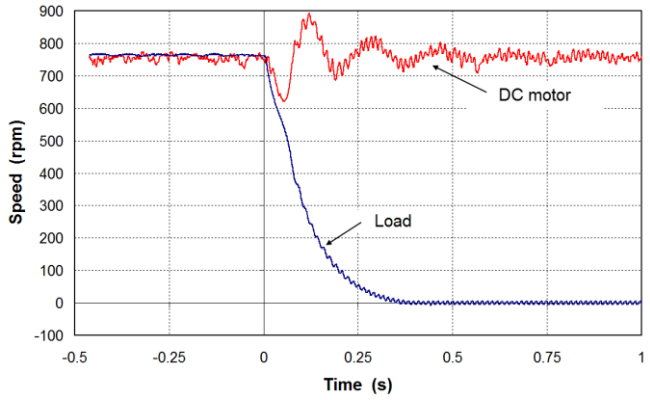

Fig. 12. Speed responses to a sudden load torque of 13.5Nm (experimental results, e = 20mm), synchronism loss.

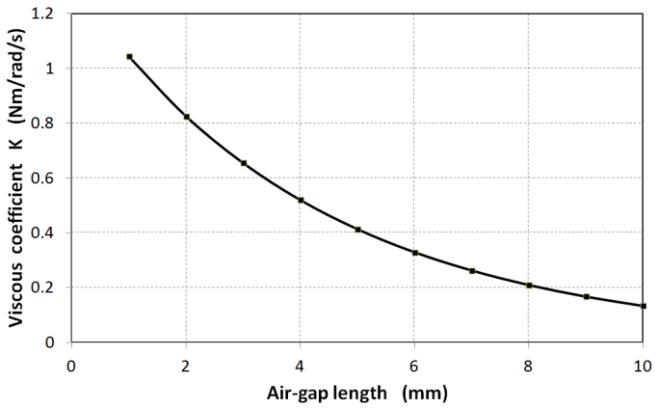

Fig. 13. Viscous coefficient K (Nm.s.rad^{-1}) versus air-gap length.

$$\begin{aligned} J_1 \frac{d\Omega_1}{dt} + (B_1 + K)\Omega_1 &= T_{DC} + K\Omega_2 \\ J_2 \frac{d\Omega_2}{dt} + (B_2 + K)\Omega_2 &= K\Omega_1 - T_{load} \end{aligned} \tag{11}$$

We can observe that the impact on the motion equations is absolutely not the same for the eddy-current coupling compared to the synchronous coupling (10). While the synchronous coupling adds an additional torsional stiffness in the motion equation, the eddy-current coupling adds an additional viscous damping coefficient and the impact on the

speed response is totally different as it will be shown.

In order to show the impact of the eddy-current coupling on the transient performance, we first consider the response to a start-up. The DC motor starts from standstill to 400 rpm in steady-state condition. Figure 14 compares the speed response obtained with the analytical model (11) with the measurement. We can observe that a delay time exists for the speed between the two rotors. Because of the no-load condition, the speed value in steady state is almost identical on both sides of the coupling (a little speed difference can be observed in Fig. 14). It is worth noting that no oscillation appears on the speed responses during the transient, as it was for synchronous coupling with permanent magnets on both sides (Fig. 10). An advantage of eddy-current couplings compared to synchronous couplings is that it is torque ripple free [24], and can be used as vibration isolation system.

The transient performance of the eddy-current coupling for a sudden application of load torque is now studied and the results are given in Fig. 15. Before the load torque is applied, the DC motor is in steady-state condition and runs with a speed of 750 rpm under no-load condition. At t = 0s, a load torque is applied. After a transient of around 0.6s, the two rotors are once again in steady state but the speed is not the same on the two sides of the coupling as it was for the synchronous coupling (fig. 11).

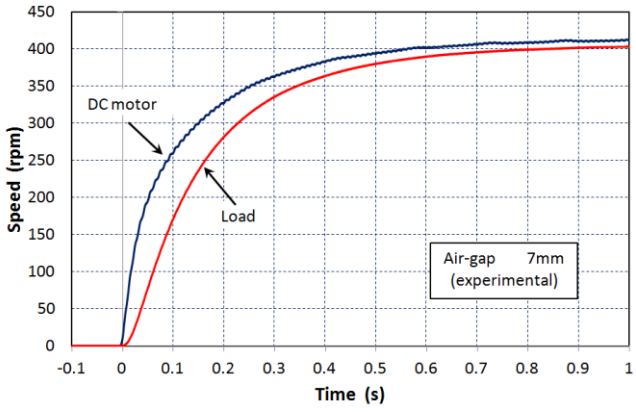

(a)

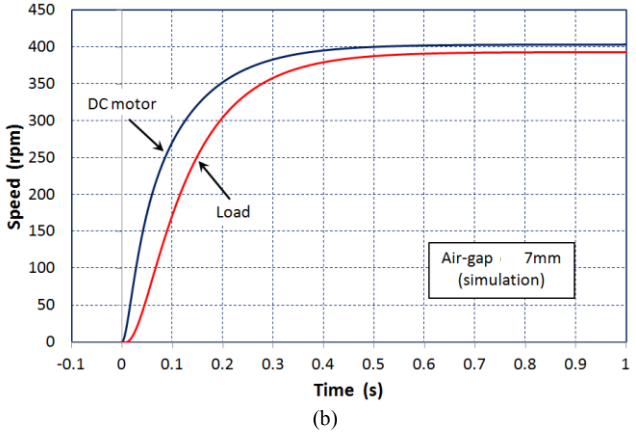

(b)

Fig. 14. Speed response for the eddy-current coupling (e = 7mm): (a) experimental result, (b) simulation result.

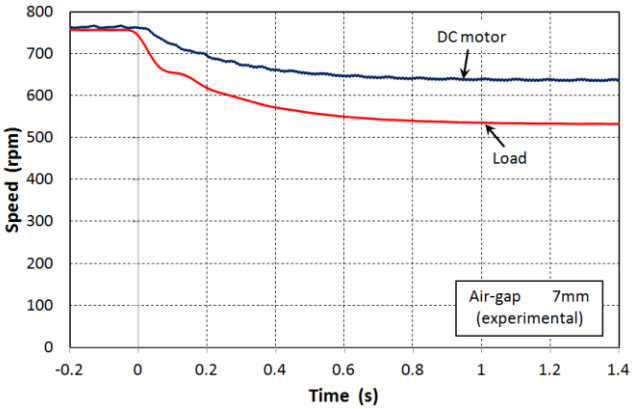

Fig. 15. Speed response to a sudden load torque for the eddy-current coupling.

With the eddy-current coupling, a certain amount of speed is lost between the input and the output. This difference increases with the torque transmitted as shown in Fig. 7. This leads to additional losses (Joule losses in the copper) which impact the global efficiency of the system. It is well known that the efficiency of the eddy-current coupling is given by $\eta = 1-s$ where s is the slip ($s = \Omega/\Omega_1$).

If the load torque is greater than the maximum transmissible torque (overload condition), the load side of the magnetic coupling will stop. In this case, the eddy-current magnetic coupling acts as a brake, with a rapid increase of the copper plate temperature.

IV. Conlusion

In this paper, we have compared the transient performances of synchronous and eddy-current magnetic coupling. We have proposed simple but effective torque formulas for each magnetic coupling. The proposed models can predict both the steady-state and the transient performances with good accuracy. Experimental results have shown that the use of a synchronous coupling in a mechanical transmission causes speed oscillations during start-up, whereas it is not the case for the eddy-current coupling. On the other hand, eddy-current coupling causes speed difference between input and output during the steady-state, with additional losses that impact the global efficiency of the system.

Eddy-current coupling presents good performance during the transient (no speed oscillation) and synchronous coupling good performance during the steady state (driven speed equal driving speed, no loss). Finally, a possible solution is to add a copper part (damper) to the synchronous coupling in order to improve its performance during the transient like it has been done recently for magnetic gear [10].

V. References

[1] R. M. Hornreich and S. Shtrikman, "Optimal design of synchronous torque couplers," *IEEE Trans. Magn.*, vol. 14, no. 5, pp. 800–802, Sept. 1978.

[2] E. P. Furlani, "Formulas for the force and torque of axial couplings," *IEEE Trans. Magn.*, vol. 29, no. 5, pp. 2295–2301, Sept. 1993.

[3] J. P. Yonnet, S. Hemmerlin, E. Rulliere, and G. Lemarquand, "Analytical calculation of permanent magnet couplings," *IEEE Trans. Magn.*, vol. 29, no. 6, pp. 2932–2934, Nov. 1993.
[4] J. F. Charpentier and G. Lemarquand, "Optimal design of cylindrical air-gap synchronous permanent magnet couplings," IEEE Trans.*Magn.*, vol. 35, no. 2, pp. 1037–1046, Mar. 1999.
[5] C. Ferreira and J. Vaidya, "Torque analysis of permanent magnet coupling using 2D and 3D finite elements methods," *IEEE Trans. Magn.*, vol. 25, pp. 3080–3082, Jul. 1989.
[6] T. Lubin, S. Mezani, and A. Rezzoug, "Simple analytical expressions for the force and torque of axial magnetic couplings*," IEEE Trans. Energy. Convers.,* vol. 27, no. 2, pp. 536-546, Jun. 2012.
[7] W. Wu, H. C. Lovatt, and J. C. Dunlop, "Analysis and design optimisation of magnetic couplings using 3D finite element modelling," *IEEE Trans. Magn.*, vol. 33, no. 5, pp. 4083–4085, Sept. 1997.
[8] K. T. Chau, D. Zhang, J. Z. Jiang, and L. Jian, "Transient analysis of coaxial magnetic gears using finite element comodeling*," J. Appl. Phys.,* vol. 103, 07F101, 2008.
[9] J. Fontchastagner, Y. Lefèvre and F. Messine, "Some Co-axial Magnetic Couplings Designed Using an Analytical Model and an Exact Global Optimization Code," *IEEE Trans. Magn.*, vol. 45, no. 3, pp 1458-1461, Mar. 2009.
[10] N. W. Franck, S. Pakdelian, and H. A. Toliyat, "Passive suppression of transient oscillations in the concentric planetary magnetic gear*," IEEE Trans. Energy. Convers.,* vol. 26, no. 3, pp. 933-939, Sept. 2011.
[11] R. G. Montague, C. M. Bingham, and K. Atallah, "Servo control of magnetic gears*," IEEE/ASME Trans. Mechatronics.,* vol. 17, no. 2, pp. 269-278, Apr. 2012.
[12] J. Fontchastagner, T. Lubin, F. Messine, and S. Mezzani, "Efficient Design Using Successive Analytical Subproblems Method: Application to Axial Magnetic Couplings," *IEEE Trans. Magn.*, vol. 51, no. 3, pp. 1-4, Mar. 2015.
[13] T. Lubin, S. Mezani, and A. Rezzoug, "Experimental and theoretical analyses of axial magnetic coupling under steady-state and transient operation", *IEEE Trans. Ind. Electron.*, vol. 61, no. 8, pp.4356 -4365, Aug. 2014.
[14] B. Dolisy, S. Mezani, T. Lubin, and J. Lévêque, "A new analytical torque formula for axial field permanent magnets coupling," *IEEE Trans. Energy Convers.*, vol. 30, no. 3, pp.892 -899, Sep. 2015.
[15] E. J. Davies, "An experimental and theoretical study of eddy-current couplings and brakes," *IEEE Transactions on Power Apparatus and Systems*, vol. 82, no. 67, pp. 401-419, August 1963.
[16] E. J. Davis, M. T. Wright, and R. C. Jonhson, "Transient performance of eddy-current couplings," *Proc. IEE,* vol. 122, no. 10, pp. 1128-1136, Oct. 1975.
[17] T. W. Nehl, B. Lequesne, V. Gangla, S. A. Gutkowski, M. J. Robinson, and T. Sebastian, "Nonlinear two-dimensional finite element modeling of permanent magnet eddy current couplings and brakes," *IEEE Trans. Magn.,* vol.30, no.5, pp. 3000-3003, Sep. 1994.
[18] A. Canova, and B. Vusini, "Analytical modeling of rotating eddy-current couplers", *IEEE Trans. Magn.,* vol. 41, no. 1, pp. 24-35, Jan. 2005.
[19] J. Wang, H. Lin, S. Fang, and Y. Huang, "A general analytical model of permanent magnet eddy current couplings," *IEEE Trans. Magn.*, vol. 50, no. 1, pp., Jan. 2014.
[20] S. Mohammadi, M. Mirsalim, and S. Vaez-Zadeh, "Non-linear modeling of eddy-current couplers," *IEEE Trans. Energy Convers.*, 2013 vol. 29, no. 1, pp. 224–231, Mar. 2014.
[21] T. Lubin, and A. Rezzoug, "Steady-state and transient performance of axial-field eddy-current coupling," *IEEE Trans. Ind. Electron.*, vol. 62, no. 4, pp. 2287–2296, Apr. 2015.
[22] Z. Mouton, and M. J. Kamper, "Modeling and Optimal Design of an Eddy Current Coupling for Slip-Synchronous Permanent Magnet Wind Generators," *IEEE Trans. Ind. Electron.*, vol. 61, no. 7, pp. 3367–3376, Jul. 2014.
[23] N. Amati, A. Tonoli, A. Canova, and M. Padovani, "Dynamic behaviour of torsional eddy-current dampers: sensitivity of the design parameters," *IEEE Trans. Magn.*, vol. 43, no. 7, pp. 3266–3277, Jul. 2007.
[24] P. Bouwer, J.H.J. Potgieter and M.J. Kamper, "Modelling and dynamic performance of a direct-drive direct-grid slip permanent magnet wind generator", IEEE (IEMDC 2011), Niagara Falls (Canada), 15-18 May, 2011, pp 137-142.
[25] T. Lubin and A. Rezzoug, "3-D analytical model for axial-flux eddy-current couplings and brakes under steady-state conditions," *IEEE Trans. Magn.,* vol. 51, no. 10, # 8203712, Oct. 2015.
[26] R. L. Russell and K. H. Norsworthy, "Eddy currents and wall losses in screened-rotor induction motors", *Proc. IEE,* vol. 105, no. 20, pp. 163-175, Apr. 1958.

VI. BIOGRAPHIES

Thierry Lubin received the M.Sc. degree from the University Pierre et Marie Curie, Paris 6, France in 1994 and the Ph.D. degree from the University Henri Poincaré, Nancy, France, in 2003. He is currently an associate professor of electrical engineering at the University of Lorraine, at the Groupe de Recherche en Electrotechnique et Electronique de Nancy (GREEN). His interests include analytical modeling of electrical devices, contactless torque transmission systems, modeling and control of synchronous reluctance motors, and applied superconductivity in electrical engineering.

Julien Fontchastagner received the Dipl. Ing. degree from the École Nationale Supérieure d'Électronique, d'Électrotechnique,d'Informatique, d'Hydraulique et desTélécommunication, Toulouse, France, and the M.Sc. degree from the National Polytechnic Institute of Toulouse in 2003, and the Ph.D. degree from Toulouse University, in 2007, all in electrical engineering. He is currently with the Groupe de Recherche en Électrotechnique et Électronique de Nancy (GREEN), Université de Lorraine, as an associate professor, where he works on solving inverse problems for electrical device design.

Smail Mezani received the Dipl.-Ing. and Magister degrees in electrical engineering from the University of Sciences and Technology Houari Boumediene, Algeria, in 1996 and 1999, respectively, and the Ph.D. degree from the Institut National Polytechnique de Lorraine, Nancy, France, in 2004. He is currently an associate professor in Electrical Engineering, Université de Lorraine, Nancy, where he is involved in research with the Groupe de Recherche en Électrotechnique et Électronique de Nancy. His current research interests include numerical and analytical modeling of electrical machines and contactless torque transmissions, coupled magnetic and thermal problems, and the applications of superconductors in electromechanical devices

Abderrezak Rezzoug received the electrical engineer degree from ENSEM, Institut National Polytechnique de Lorraine (INPL), Nancy, France, in 1972, and the Dr. Ing. diploma and the Ph.D. degree from INPL in 1979 and 1987, respectively. He was an Assistant Professor with INPL until 1991. Afetr 20 years as Full Professor, he is currently a Professor Emeritus with the University of Lorraine, Nancy. As a member of the Groupe de Recherche en Electrotechnique et Electronique de Nancy, his main subjects of research concern superconducting applications to electrical devices and electrical machines.